AGU ADVANCING EARTH AND SPACE SCIENCES

JGR Atmospheres

RESEARCH ARTICLE
10.1029/2025JD045776

Rossby Wave Breaking Driving Desert Extreme Precipitation in the UAE During April 2024

Jinxia Zhang[1], Shanshan Wang[1,2], Jianping Huang[1,2], Xinya Shu[1], Hao Wang[1], Yongli He[1,2], Fei Ji[1,2], and Shanjun Cheng[3]

[1]Key Laboratory for Semi-Arid Climate Change of the Ministry of Education, College of Atmospheric Sciences, Lanzhou University, Lanzhou, China, [2]Collaborative Innovation Center for Western Ecological Safety, Lanzhou University, Lanzhou, China, [3]Tianjin Climate Center, Tianjin, China

Key Points:

- Rossby wave breaking is a crucial physical mechanism driving the desert extreme precipitation in the UAE
- Warmer temperatures over the North Atlantic–Mediterranean and Eastern Europe trigger the Rossby waves
- The Middle East jet, Arabian low vortex, and subtropical high are dominant synoptic systems directly influencing the desert rainstorms

Supporting Information:

Supporting Information may be found in the online version of this article.

Correspondence to:

S. Wang and J. Huang,
wangss@lzu.edu.cn;
hjp@lzu.edu.cn

Citation:

Zhang, J., Wang, S., Huang, J., Shu, X., Wang, H., He, Y., et al. (2026). Rossby wave breaking driving desert extreme precipitation in the UAE during April 2024. *Journal of Geophysical Research: Atmospheres*, *131*, e2025JD045776. https://doi.org/10.1029/2025JD045776

Received 31 OCT 2025
Accepted 8 APR 2026

Abstract An unprecedented extreme precipitation event struck the hyper-arid United Arab Emirates (UAE) and surrounding regions in mid-April 2024, severely disrupting infrastructure and public life. However, few studies pay attention to desert rainstorms. This study identifies Rossby wave breaking as the key dynamic mechanism underlying the extreme events. The pronounced positive sea surface temperature anomalies over the eastern North Atlantic–Mediterranean and land surface temperature anomalies over Eastern Europe acted as remote thermal forcings, triggering Rossby waves that propagated downstream and broke over the Arabian Peninsula, leading to enhanced upper-level divergence and dynamically induced ascent that contributed to the event. Specifically, the disruption of the Middle East jet at 200 hPa enhanced upper-tropospheric divergence, while strong convergence of southwest winds ahead of the Arabian vortex and southeast winds west of the subtropical high at 500 hPa promoted upward motion and moisture transport over the UAE. These findings emphasize the crucial role of remote ocean-atmosphere and land-atmosphere interactions in shaping extreme precipitation in arid regions and provide insights for improving forecasting and risk mitigation.

Plain Language Summary The United Arab Emirates (UAE) is known for its hot, dry desert climate and is highly vulnerable to rare extreme precipitation. In April 2024, an exceptionally intense rainstorm hit the UAE and nearby areas. Some areas received more than a year's worth of rain in just 1 day, leading to flooding, fatalities, and major disruptions to daily life. What caused such an unusual event? Our research shows that abnormal changes in ocean and land temperatures, especially over the North Atlantic, Mediterranean, and Eastern Europe, played a key role. These changes disrupted the wind field in the atmosphere, setting off waves that traveled thousands of kilometers. When these waves broke over the Arabian Peninsula, they released energy that caused strong upward air movement and moisture convergence, producing heavy rainfall. This study shows how weather events in one part of the world can be influenced by distant regions, and it helps us better understand extreme weather in dry areas such as the UAE.

1. Introduction

In recent decades, frequent natural disasters driven by extreme climate events, such as floods, droughts, heat-waves, rainstorms, and cold waves, have significantly threatened both socioeconomic structures and natural ecosystems (AghaKouchak et al., 2020; Gong et al., 2024). Recent data show that these extreme weather and climate events have caused nearly 1.6 million fatalities and over $4.6 trillion in economic losses worldwide over the past four decades (Ferreira, 2024; W. Zhang & Zhou, 2020). To date, while numerous studies have extensively investigated extreme precipitation events across various global regions, including East Asia, South Asia, North America, and Europe (Duan et al., 2023; Hsu et al., 2023; Suman & Maity, 2020; Sun et al., 2021; Yang et al., 2019; Zeder & Fischer, 2020), arid and semi-arid regions have received comparatively less attention. These regions, covering more than a quarter of Earth's terrestrial surface, exhibit pronounced intermittent hydrological conditions and have experienced an increasing frequency of severe precipitation events in recent years (Donat et al., 2016; J. Zhang et al., 2023). Moreover, sparse vegetation and inadequate drainage systems in these arid environments mean that extreme precipitation is more likely to result in catastrophic events, posing significant threats to development efforts (Guan et al., 2023; Guan & Huang, 2024; J. Huang, Li, et al., 2017). For instance, on 16 April 2024, the UAE and northern Oman, typically characterized by a hyper-arid desert climate, experienced extraordinarily intense rainfall (https://www.ecmwf.int/en/newsletter/180/news/unprecedented-rainfall-united-arab-emirates). Numerous meteorological stations recorded rainfall exceeding 100 mm, equivalent to

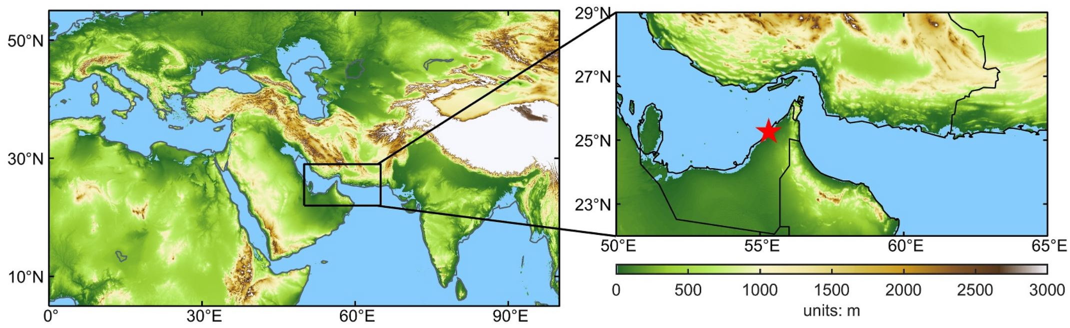

Figure 1. Topography and location of the study region. The color shading indicates the terrain elevation; blue shading denotes ocean areas. The study region (22–29°N, 50–65°E) is outlined by a black rectangle on the left panel, and Dubai is marked by a red star on the right.

1.5 years of the region's average annual precipitation, with the highest 24-hr rainfall reaching 259.5 mm, setting a new record since meteorological records began in 1949. This extreme rainfall severely disrupted infrastructure and public life, leading to at least 20 fatalities in Oman and four in the UAE. As a major oil-exporting nation and a hub of global travel networks, the hyper-arid UAE is vulnerable to extreme weather events. This event highlighted the broader implications of climate change on global trade and economic activities and has sparked renewed attention and discussion (Almheiri et al., 2024; Nyarko, 2024). However, the weather and climatic causes behind these desert rainstorms remain insufficiently explored.

Located in the northeastern Arabian Peninsula along the Persian Gulf, the UAE features flat deserts along the coast and mountains in the east reaching over 1,500 m (Figure 1). It experiences a hyper-arid desert climate, with annual precipitation ranging from 40 mm in deserts to 160 mm in mountains, and an overall mean of approximately 78 mm. This precipitation is highly variable both seasonally and interannually, with standard deviation sometimes exceeding the mean annual rainfall (Chowdhury et al., 2016; Niranjan Kumar & Ouarda, 2014; Ouarda et al., 2014). In summer, the UAE is influenced by upper-level easterly to northeasterly winds, which are linked to the tropical easterly belt and a thermal low over the sub-Asian regions (Niranjan Kumar & Ouarda, 2014). This atmospheric circulation can transport moisture from the Arabian Sea but is moderated by subsiding air from a subtropical high-pressure system, resulting in hot, humid summers with limited rainfall (Ouarda et al., 2014; Renwick et al., 2015). In winter, a southward shift of the subtropical high-pressure belt exposes the UAE to subtropical westerlies, accompanied by the intrusion of low-pressure troughs, cyclonic systems, and frontal systems from the west and northwest, creating favorable conditions for precipitation in the UAE (Niranjan Kumar et al., 2016; Rana et al., 2018). These rainfall-bearing systems predominantly originate from the Atlantic and Mediterranean regions, and their development and eastward propagation are typically affected by large-scale circulation conditions associated with several teleconnection factors (Francis et al., 2024; Niranjan Kumar & Ouarda, 2014).

Numerous studies have examined the impact of global sea surface temperature (SST), especially from the North Atlantic and Tropical Pacific, on precipitation patterns in the UAE and surrounding areas. Evidence indicates that teleconnections such as the El Niño–Southern Oscillation (ENSO) and the North Atlantic Oscillation (NAO) have shown significant influence. Based on canonical correlation analysis, Niranjan Kumar and Ouarda (2014) and Rana et al. (2018) indicate that precipitation in the Arabian Peninsula and the surrounding regions is primarily predictable from Pacific SST variations linked to ENSO and the Pacific Decadal Oscillation (PDO). Cold (warm) ENSO conditions, combined with cold (warm) PDO phases, induce a northward (southward) shift of the subtropical jet stream, leading to negative (positive) precipitation anomalies. During El Niño years, moisture transport from the Red and Arabian Seas toward the Arabian Gulf intensifies, while it weakens during La Niña and neutral years, with most transport directed toward the northern Arabian Gulf (Sandeep & Ajayamohan, 2018). In addition, existing studies suggest that the NAO modulates precipitation and temperature in the Middle East from December to March on interannual to decadal timescales, notably increasing precipitation during its negative phase by enhancing heat and moisture fluxes from the Atlantic (Cullen et al., 2002). The negative phase of the NAO is linked to stronger zonal surface winds and storm tracks across the North Atlantic, resulting in warmer and wetter winters in the Mediterranean and the Middle East (Aizen et al., 2001; Cullen &

deMenocal, 2000). These teleconnection processes, primarily driven by anomalous surface temperatures, underscore the critical role of surface temperature anomalies in shaping precipitation patterns over the UAE.

While past research has mainly focused on the impact of these teleconnection factors on both seasonal and annual precipitation, the specific mechanisms of extreme precipitation events in the UAE and nearby regions need further exploration. Given the hyper-arid nature of this region, even a single extreme rainfall event can serve as a natural experiment that provides valuable insight into the underlying physical processes. Additionally, during the record-breaking precipitation in the UAE in 2024, anomalously high SST and land surface temperatures (LST) were observed in the eastern North Atlantic, Mediterranean, and Eastern Europe (https://www.ncei.noaa.gov/access/monitoring/ghcn-gridded-products/maps/202404). Understanding how these remote anomalies influence such extreme events and their underlying mechanisms is crucial. This study aims to enhance understanding of this extreme event and provide valuable insights into the combined effects of SST and LST on extreme weather in the UAE. Furthermore, although the present work focuses on a single record-breaking case, the physical framework revealed by this study may be applicable to other midlatitude arid and semi-arid regions, contributing to improved forecasting and more effective disaster mitigation strategies.

The manuscript is organized as follows. The data and related methods employed in this study are provided in Section 2. Section 3 begins by presenting the observed extreme precipitation events and the associated atmospheric circulation anomalies. We then examine the influence of Rossby waves triggered by anomalous SST and LST on rainfall patterns over the UAE. Finally, we explore the underlying physical mechanisms that govern the extreme precipitation induced by the breaking of Rossby waves. Section 4 provides the conclusions and discussions of the study.

2. Data and Methods

2.1. Data

ERA5, a state-of-the-art atmospheric reanalysis data set from the European Centre for Medium-Range Weather Forecasts (ECMWF) (Hersbach et al., 2020), offers high-resolution global data from 1940 to the present. It is extensively used in climate and weather research, providing valuable insights into long-term trends and extreme events (S. H. Huang et al., 2022; Nie & Sun, 2022; W. Zhang et al., 2024). Given the sparse distribution of observational stations in the arid and semi-arid regions of the Middle East and surrounding areas, ERA5 was selected in this study, as it outperforms other reanalysis data sets in the region (Fonseca et al., 2021; Francis et al., 2024; Nelli et al., 2021; Taraphdar et al., 2021). To verify the reliability of ERA5 precipitation, we compared it with satellite-based products (GPM and CMORPH), and the results showed good consistency among the three data sets in terms of spatial distribution and temporal evolution of this event (Figure S1 in Supporting Information S1). Consequently, hourly and monthly data on precipitation, temperature, wind, geopotential height, vertically integrated water vapor flux and divergence, and vertical velocity from 1951 to 2024, with a horizontal resolution of 0.25° × 0.25° and 37 vertical levels, were extracted from ERA5 for the analysis of the extreme precipitation events and atmospheric circulation anomalies. Additionally, daily outgoing longwave radiation data from ERA5 were utilized to assess the convective activity associated with extreme precipitation events. Moreover, LST data from ERA5-land and SST from the Extended Reconstructed Sea Surface Temperature, version 5 (ERSST.v5) (B. Huang, Thorne, et al., 2017) were employed to examine the Rossby waves induced by anomalous surface temperature. To further investigate the propagation and breaking of Rossby waves, hourly potential vorticity (PV) data from ERA5 were also used.

2.2. Wave Activity Flux

The propagation of Rossby waves is typically diagnosed through wave activity flux (WAF; units: m^2/s^2) in the field of atmospheric dynamics. To investigate the evolution characteristics of Rossby waves triggered by anomalous surface temperatures, this study applied the WAF method proposed by Takaya and Nakamura (2001). The horizontal WAF is calculated based on the following formula:

$$\mathrm{WAF} = \frac{p\cos\varphi}{2|\boldsymbol{U}|}\begin{bmatrix} \frac{u}{a^2\cos^2\varphi}\left(\psi_x'^2 - \psi'\psi_{xx}'\right) + \frac{v}{a^2\cos\varphi}\left(\psi_x'\psi_y' - \psi'\psi_{xy}'\right) \\ \frac{u}{a^2\cos\varphi}\left(\psi_x'\psi_y' - \psi'\psi_{xy}'\right) + \frac{v}{a^2}\left(\psi_y'^2 - \psi'\psi_{yy}'\right) \end{bmatrix} \tag{1}$$

where $\boldsymbol{U} = (u, v)$ represents the climatological mean of the horizontal wind field, with u as the zonal wind and v as the meridional wind (units: m/s), which is calculated over the period from 1991 to 2020; φ denotes latitude (units: rad); a is the radius of the Earth (units: m); p represents pressure (units: hPa), scaled by 1,000 hPa; and ψ' represents the perturbation stream function under the quasi-geostrophic approximation (units: m^2/s). Subscripts x and y represent the longitudinal and latitudinal derivatives, respectively.

2.3. Rossby Wave Source

The Rossby wave source (RWS; units: s^{-2}) was employed to examine the generation mechanisms of Rossby waves. Based on the barotropic vorticity equation, an anomalous vorticity source, S', is described as follows (Sardeshmukh & Hoskins, 1988):

$$S' = -\nabla\cdot(\boldsymbol{v}_\chi\zeta)' \tag{2}$$

where $\boldsymbol{v}_\chi$ signifies the divergent component of the horizontal wind field (units: m/s), ζ denotes absolute vorticity (units: s^{-1}), and the prime indicates anomaly. Following Sekizawa et al. (2021), S' is linearized as:

$$S' = S_1 + S_2 + S_3 + S_4 = -\bar{\zeta}\nabla\cdot\boldsymbol{v}_\chi' - \boldsymbol{v}_\chi'\cdot\nabla\bar{\zeta} - \zeta'\nabla\cdot\bar{\boldsymbol{v}}_\chi - \bar{\boldsymbol{v}}_\chi\nabla\zeta' \tag{3}$$

where the overbar denotes the climatological mean value. S_1 and S_3 are vortex stretching terms, representing the effect of anomalous divergence on climatological absolute vorticity and the effect of climatological divergence on anomalous absolute vorticity, respectively; S_2 and S_4 are vorticity advection terms, arising from regions with a strong vorticity gradient, accounting for the advection of climatological absolute vorticity by anomalous divergent winds and the advection of anomalous absolute vorticity by climatological divergent winds, respectively. In this study, we calculated the sum of the four terms, noting that the first term (S_1) dominates the RWS.

2.4. Rossby Waves Breaking

Rossby waves breaking (RWB) is characterized by the irreversible distortion of material contours, arising from the amplification of Rossby waves in areas with weaker zonal flow or diffluence (McIntyre and Palmer, 1983, 1985). Typically, RWB at the terminal phase of the wave cycle is linked to intrusions of high-PV air into the tropopause. Therefore, the analysis of meridional overturning of PV on specific isentropic or isobaric surfaces can be employed to identify RWB, and these overturned PV contours generally exhibit a tongue-like structure (Allen et al., 2008; Biyo et al., 2024; Nielsen-Gammon, 2001). In this study, we quantitatively identified RWB using the Streamer Index implemented in the WaveBreaking Python package (https://wavebreaking.readthedocs.io; Sprenger et al., 2017; Wernli & Sprenger, 2007). The algorithm computes for every pair of contour points: the great-circle distance D and the along-contour path length L. A pair is flagged as a streamer basepoint when $D < 800$ km and $L > 1{,}500$ km, indicating two points that are geographically close but far apart along the contour. The algorithm then constructs polygons for the regions enclosed by the contour and the geodesic connection, which are returned as PV streamers. For this analysis, we focus on PV contours at 250 hPa from the daily ERA5 data and apply a threshold of 2 potential vorticity units (PVU; 1 PVU = 10^{-6} K·m^2·kg^{-1}·s^{-1}) to identify PV streamers, as this value represents the dynamic tropopause in mid-latitude regions and effectively captures strong PV intrusions over the subtropical Arabian Peninsula.

2.5. Dynamic Recycling Model

Sufficient water vapor is a necessary condition for the formation of extreme precipitation. To quantitatively investigate the moisture sources and transport pathways associated with this extreme rainfall event, we applied the Dynamic Recycling Model (DRM; Dominguez et al., 2006, 2020). DRM is a diagnostic tool based on reanalysis data that tracks the transport pathways and cycling processes of atmospheric moisture, thereby identifying the

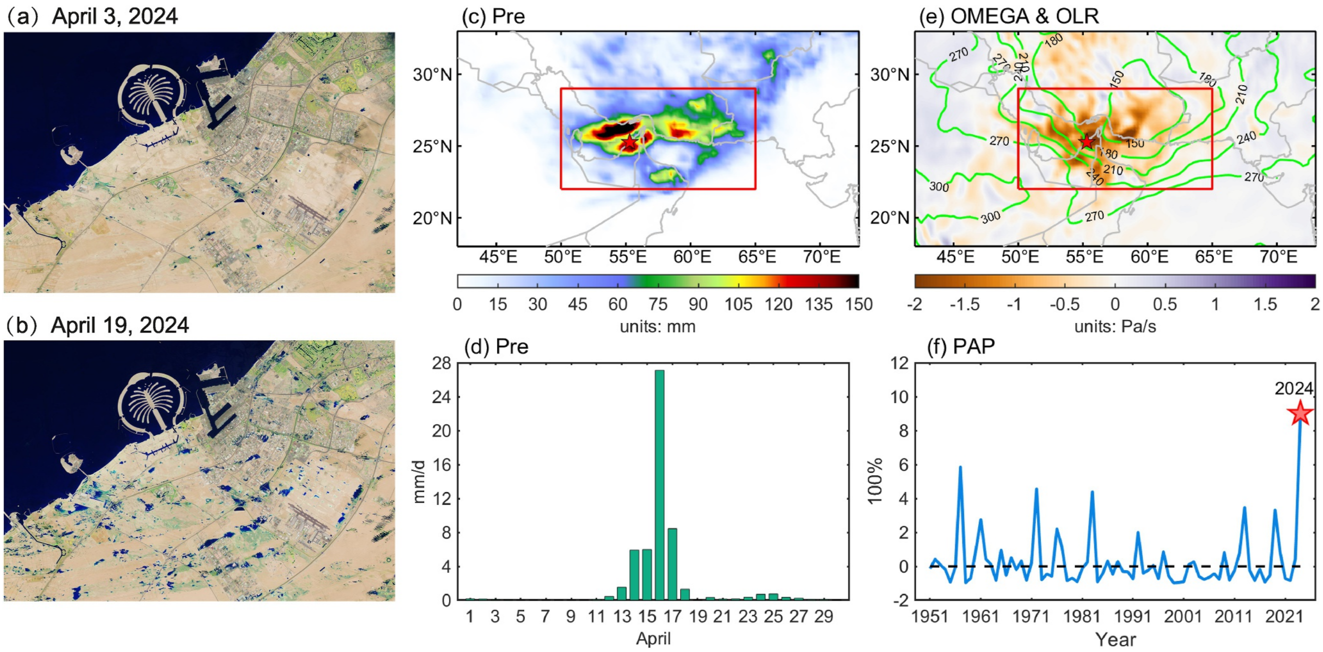

Figure 2. The record-breaking extreme Precipitation event over the UAE in April 2024. Satellite Images of (a) 3 April 2024 (b) 19 April 2024 acquired with the satellite's OLI-2 (Operational Land Imager 2) when Landsat 9 passed over the Jebel Ali (The Satellite Images are available at https://earthobservatory.nasa.gov/images/152703/deluge-in-the-united-arab-emirates). Blue emphasizes the presence of water. (c) Total precipitation (Pre; units: mm) from 14 to 17 April 2024. (d) Daily precipitation (Pre; units: mm/d) in April 2024 averaged over the region of 22–29°N, 50–65°E (red box in c). (e) Vertical velocity at 500 hPa (OMEGA; shading; units: Pa/s) and outgoing longwave radiation (OLR; contour; units: W/m^2) on 16 April 2024. (f) Time series of the April precipitation anomaly percentage (PAP; units: %) over the red box in (c) for 1951–2024, calculated relative to the April climatology during 1991–2020. The same 1991–2020 climatological baseline is used to define anomalies throughout the study.

main sources and transport channels of precipitation over a target region. In addition, it is computationally efficient and suitable for regional-scale applications. In this study, we selected 50–65°E and 22–29°N as the target regions and conducted a 15-day backward tracking with DRM for the period of 12–18 April 2024.

2.6. Statistical Techniques

Pearson correlation and linear regression are widely adopted as fundamental diagnostic tools in climate science to identify broad, statistically significant associations, particularly in the context of remote forcings (Shu et al., 2024; Wang et al., 2022; Wilks, 2019). The Pearson correlation coefficient quantifies the strength and direction of the linear relationship, and the technique was employed primarily to reveal the first-order linear relationship between surface temperature, atmospheric circulation, and precipitation in this study. Meanwhile, both simple linear regression and multiple linear regression were employed to model the predictive association, quantifying the impact of surface temperature anomalies on atmospheric circulation and precipitation patterns. Additionally, to further validate the linear results, we conducted composite analysis, which categorized the extreme warm and cold SST/LST events and compared the corresponding atmospheric circulation and precipitation fields.

3. Results

3.1. Extreme Precipitation in the UAE

Figures 2a and 2b display satellite images of Jebel Ali, a town situated 35 km southwest of Dubai, captured before and after the extreme rainfall event of 16 April 2024. Following the heavy rainfall, widespread flooding was observed throughout most areas of the town, particularly in the industrial zone south of Jebel Ali Port and near the green resorts and parks south of Palm Jebel Ali. Daily precipitation data indicate that this extreme event was primarily concentrated from April 14 to 17, with the peak intensity occurring on April 16 (Figure 2d). The precipitation centers were located in the northern UAE, southern Persian Gulf, and southern Iran, where the

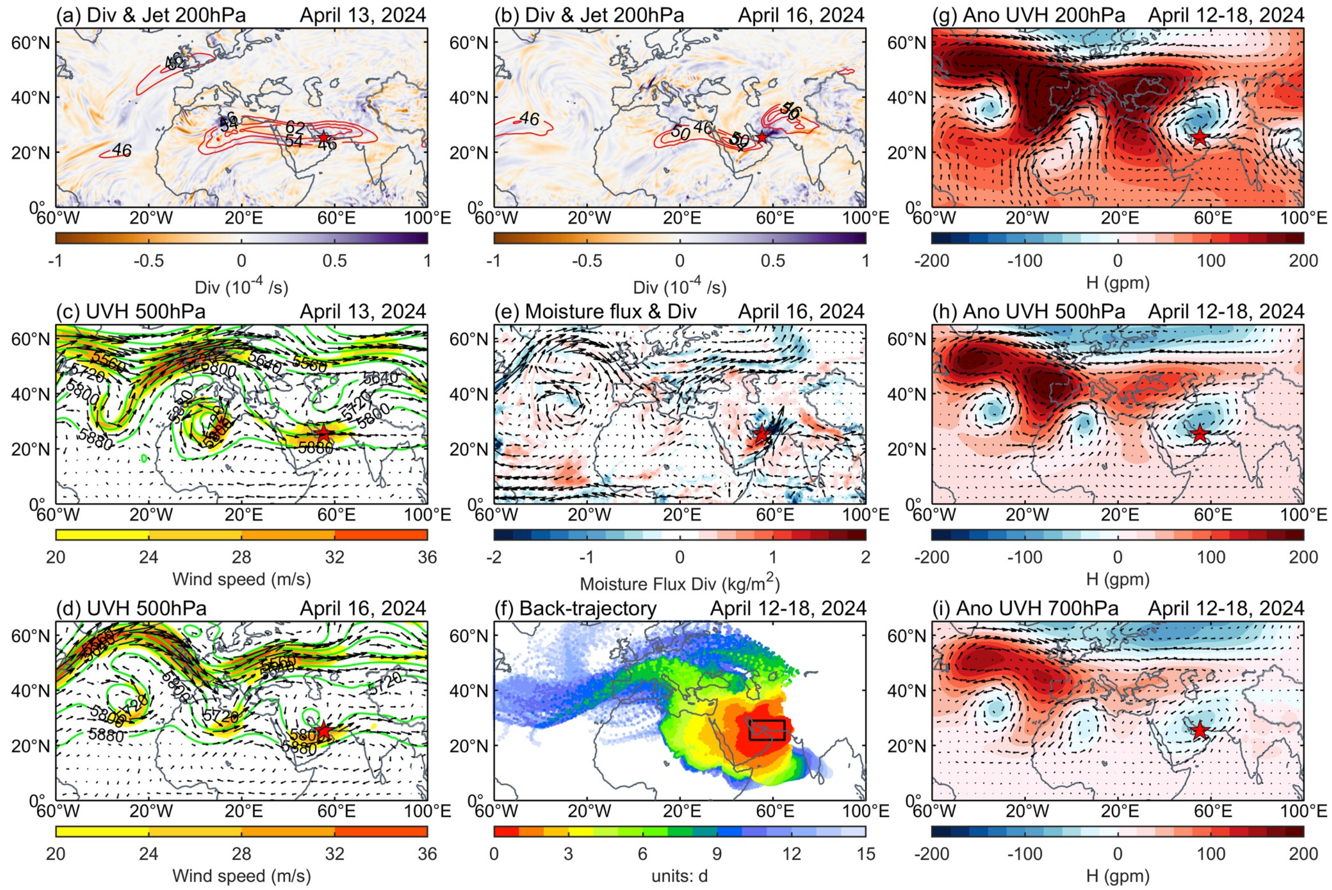

Figure 3. The atmospheric circulation during the UAE extreme precipitation event of April 2024. The spatial distribution of divergence (shading; units: 10^{-4}/s), wind speed (contour; units: m/s) at 200 hPa on April 13 (a) and 16 (b). The spatial distribution of wind field (vector), and its magnitude (shading; units: m/s) and geopotential height field (contour; units: gpm) at 500 hPa on April 13 (c) and 16 (d). (e) The vertically integrated moisture flux (vector) and divergence (shading; units: kg/m^2) on 16 April 2024. (f) 15-day moisture back-trajectory of the extreme precipitation during the period of 12–18 April 2024. (g) The distribution of wind filed (vector) and geopotential height field (shading; units: gpm) anomaly at 200 hPa during 12–18 April 2024, relative to the climatological mean in April of 1991–2020. Panels (h) and (i) are the same as (g) but for 500 and 700 hPa, respectively.

intensity exceeded 150 mm (Figure 2c). This extreme precipitation was facilitated by the favorable upward motion and strong convective activity, with the maximum upward velocity reaching −2 Pa/s, as indicated by the vertical velocity and outgoing longwave radiation analyses for April 16 (Figure 2e). When comparing this record-breaking extreme precipitation event with historical data from the same period, the maximum precipitation anomaly percentage (PAP) for April 2024 in the UAE and surrounding regions exceeded 3,000% (Figure S2 in Supporting Information S1). The regional average PAP indicates that this event was over 9 times the climatological average, marking it as the most extreme on record (Figure 2f).

Such extreme precipitation is usually associated with the favorable atmospheric circulation patterns. For this case, we found that before the onset of precipitation, the UAE was located along the axis of the 200 hPa Middle East jet stream, which extended from North Africa to northwest India (Figure 3a). At 500 hPa, a robust subtropical high extended from the Sahara Desert to the Indian Peninsula, with the UAE situated north of the subtropical high (Figure 3c). On April 16, despite a weakening of the Middle East jet stream, it bifurcated into eastern and western branches, with the UAE situated to the right of the eastern branch's entrance region and to the left of the western branch's exit region (Figure 3b). It is noteworthy that on the 16th, the values of divergence at 200 hPa over the UAE showed a marked increase, indicating enhanced upper-level divergence. This configuration intensified secondary circulation and upward motion, coinciding with the peak precipitation intensity on that day. Concurrently, in the middle troposphere, as the rainy day approached, the robust subtropical high fragmented into two separate high-pressure systems, one over the Arabian Sea (Figure 3d). A low trough embedded within the westerlies developed and deepened into the Arabian low vortex over the Arabian Peninsula. Located ahead of this

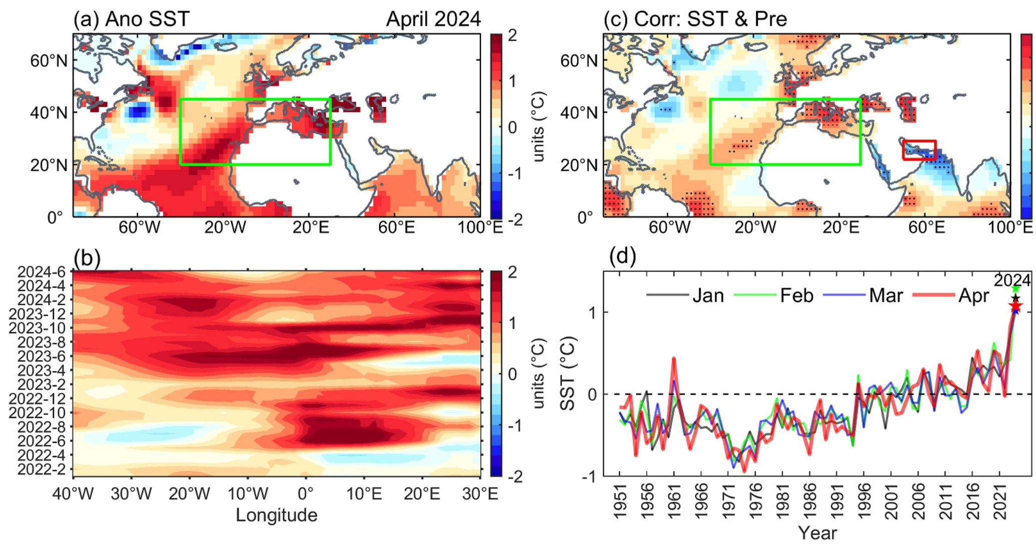

Figure 4. The anomalous SST in April 2024. (a) Distribution of the SST anomaly in April 2024, relative to the climatological mean in April of 1991–2020 (units: °C; green rectangle: 20°N–45°N, 40°W–30°E). (b) Longitude-time cross-section of the abnormal SST averaged between 20°N and 45°N over the green rectangle in (a) from January 2022 to June 2024 (units: °C). (c) The spatial distribution of the correlation coefficient between SST and precipitation averaged over the region of 22–29°N, 50–65°E (red box in c) in April from 1951 to 2024. (d) The annual variation of abnormal SST averaged over the eastern North Atlantic-Mediterranean (20°N–45°N, 40°W–30°E) for January (black), February (green), March (blue) and April (red) respectively (units: °C). The black dots indicate statistical significance exceeding the 90% confidence level in (c).

vortex and northwest of the subtropical high, the UAE experienced strong convergence between the southwest and southeast winds. The cold air from the low vortex collided with warm air from the subtropical high, resulting in substantial rainfall over the UAE. Regarding moisture conditions, the vertically integrated moisture flux and DRM results indicate that the moisture responsible for this precipitation predominantly originated from the low vortex itself, as well as from the Arabian Sea, Red Sea, and Mediterranean Sea (Figures 3e and 3f). Additional diagnostics of moisture flux at different tropospheric levels show that moisture transport is largely dominated by low-level circulation systems, while mid- and upper-level contributions are minor (Figures S3 and S4 in Supporting Information S1). A negative anomaly in moisture flux divergence over the UAE suggests that the intense convergence of moisture supplied the necessary moisture for the extreme rainfall. It is crucial to note that three distinct low-pressure systems-situated over the North Atlantic, North Africa, and the Arabian Peninsula-extended from the lower to upper troposphere (Figures 3g–3i). These low-pressure systems formed a quasi-barotropic wave train propagating eastward along the subtropical westerly jet from the upstream North Atlantic, initiated by the first intense low-pressure system, triggering extreme weather over the UAE. To investigate the underlying causes of this atmospheric circulation anomaly associated with this record-breaking extreme precipitation event, we further examine the roles of SST and LST in Section 3.2.

3.2. Atmospheric Circulation Induced by Surface Temperature Anomaly

In April 2024, SSTs in the eastern North Atlantic and Mediterranean were notably elevated compared to the climatological mean of 1991–2020, with the latter region exhibiting especially pronounced warming, reaching up to 2.0°C above normal (Figure 4a). This anomalous warming can be traced back to the summer of 2023 (Figure 4b). When compared to the historical records, SSTs in these regions from January to April 2024 were the highest since 1951 (Figure 4d). Furthermore, a correlation analysis revealed a significantly positive association between SST in the eastern North Atlantic-Mediterranean and precipitation in the UAE, with the highest correlation coefficient reaching 0.3 (Figure 4c). Similarly, LST records in 2024 show that unusual warmth began in Europe in February, migrating eastward from Western to Eastern Europe between February and April (Figure 5). Temperature anomalies peaked in April, with Eastern Europe reaching up to 6°C above normal, which ranks first in history since 1951. Correlation analysis further confirms a significantly positive correlation between LST in Eastern Europe and precipitation in the UAE and surrounding regions, with a maximum correlation coefficient of 0.4. Thus, we define the areas marked by green rectangles in Figures 4c and 5c as Key Region I (eastern North

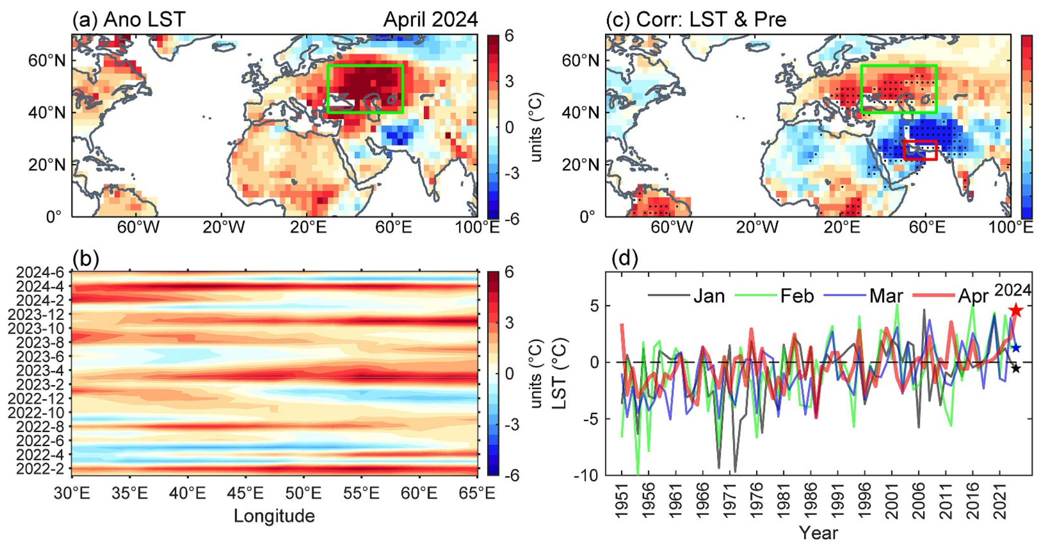

Figure 5. The anomalous LST in April 2024. (a) Distribution of the LST anomaly in April 2024, relative to the climatological mean in April of 1991–2020 (units: °C; green rectangle: 40°N–58°N, 30°E–65°E). (b) Longitude-time cross-section of the anormal LST averaged between 40°N and 58°N over the green rectangle in (a) from January 2022 to June 2024 (units: °C). (c) The spatial distribution of the correlation coefficient between LST and precipitation averaged over the region of 22–29°N, 50–65°E (red box in c) in April from 1951 to 2024. (d) The annual variation of anormal ST averaged over the Eastern Europe (40°N–58°N, 30°E–65°E) for January (black), February (green), March (blue) and April (red), respectively (units: °C). The black dots indicate statistical significance exceeding the 90% confidence level in (c).

Atlantic-Mediterranean) and Key Region II (Eastern Europe) to explore their underlying relationship with precipitation in the UAE.

Initially, we investigated the influence of anomalous SST in Key Region I and LST in Key Region II on the atmospheric circulation (Figure 6). The circulation anomaly in April 2024 displays a high-low-high-low geopotential height wave pattern, extending from the North Atlantic to Southwest Asia (Figure 6a). A large

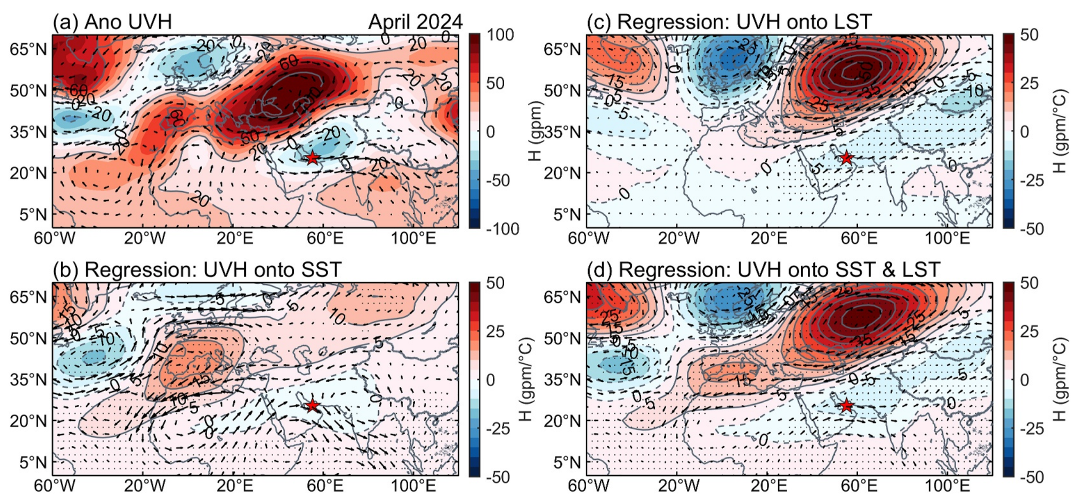

Figure 6. The influence of SST and LST on the atmospheric circulation. (a) The spatial distribution of wind filed (vector) and geopotential height field (shading; units: gpm) anomaly at 500 hPa in April 2024 relative to the climatological mean in April of 1991–2020. (b) The spatial distribution of regressions of wind filed (vector) and geopotential height field (shading; units: gpm/°C) at 500 hPa onto the April SST series over the eastern North Atlantic-Mediterranean (20°N–45°N, 40°W–30°E) during 1951–2024. Panel (c) is the same as (b) but on the April LST series over the Eastern Europe (40°N–58°N, 30°E–65° E). Similarly, panel (d) is the same as (b) but on the April SST series over the eastern North Atlantic- Mediterranean (20° N–45°N, 40°W–30°E) and the April LST series over the Eastern Europe (40°N–58°N, 30°E–65°E). The gray dots indicate statistical significance exceeding the 90% confidence level in (b)–(d).

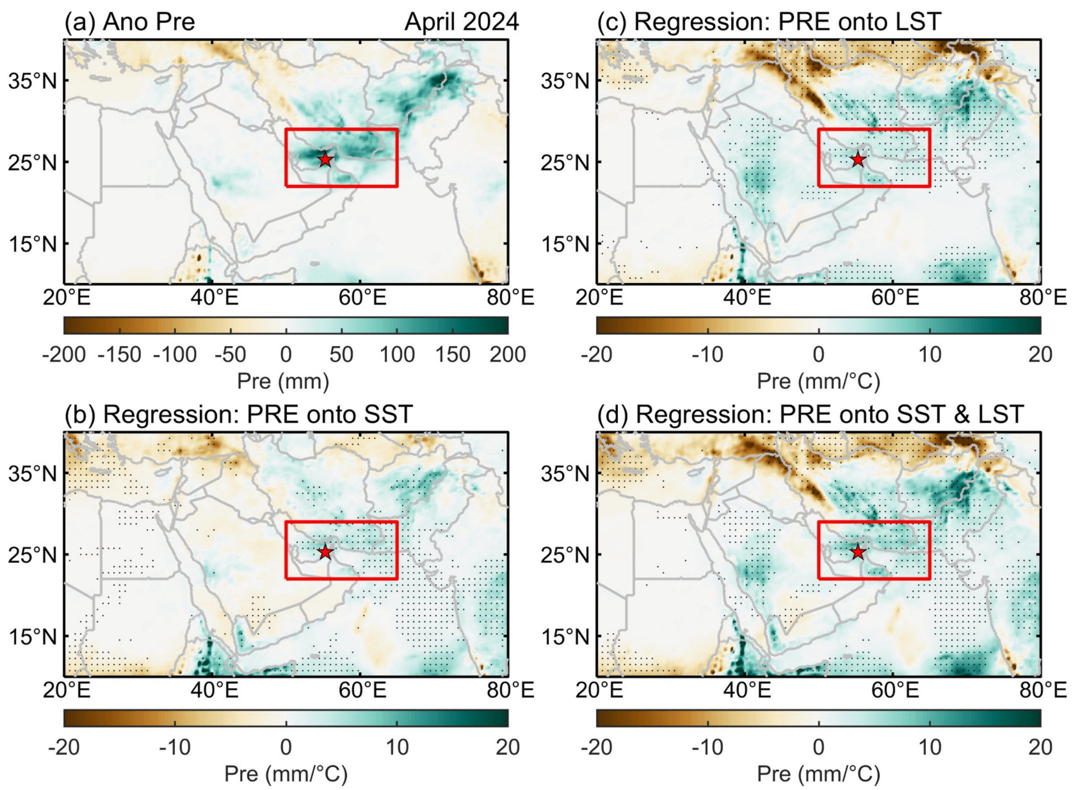

Figure 7. The influence of SST and LST on precipitation. (a) The spatial distribution of precipitation anomaly in April 2024 relative to the climatological mean in April of 1991–2020 (units: mm). (b) The spatial distribution of regression of precipitation (units: mm/°C) onto the April SST series over the eastern North Atlantic-Mediterranean (20°N–45°N, 40°W–30°E) during 1951–2024. Panel (c) is the same as (b) but on the April LST series over the Eastern Europe (40°N–58°N, 30°E–65°E). Similarly, panel (d) is the same as (b) but on the April SST series over the eastern North Atlantic-Mediterranean (20°N–45°N, 40°W–30°E) and the April LST series over the eastern Europe (40°N–58°N, 30°E–65°E). The gray dots indicate statistical significance exceeding the 90% confidence level in (b)–(d).

anomalous high-pressure system extends from the eastern North Atlantic through the Mediterranean to Eastern Europe, with its strongest center over Eastern Europe. This pattern is accompanied by a southwest-northeast oriented low-pressure belt over the North Atlantic, along with an anomalous high-pressure system west of Iceland. Notably, an anomalous low-pressure system, accompanied by an unusual cyclone, was observed over the UAE and surrounding regions, potentially leading to this unprecedented extreme precipitation event. Figures 6b and 6c show the regression of geopotential height and wind fields with the standardized, detrended SST in Key Region I and LST in Key Region II, respectively. These regression fields correspond closely with the anomalous field in April 2024, exhibiting spatial coefficients of 0.68 and 0.54, respectively, both significant at the 99% confidence level. These patterns reveal two Rossby wave trains: one extending from the eastern North Atlantic-Mediterranean to the Arabian Peninsula, and the other from Eastern Europe to the same region, consistent with the two propagation pathways identified by the WAF analysis (Figure 9). Bivariate regression further improves the spatial correlation to 0.73. This suggests that, compared to the circulation patterns generated by the individual surface temperature anomalies in Key Region I or II, the combined effects of both key regions contribute more favorable to circulation conditions for precipitation (Figure 6d). Notably, in line with the anomalies in Figure 6a, both wave trains exhibit a low-pressure cyclone over the Arabian Peninsula, suggesting in-phase superposition that merged and intensified the low-cyclone, creating favorable dynamic conditions for precipitation in the UAE. The regression fields of these two key regions on precipitation demonstrate that both regions exert a positive influence on precipitation in the UAE and surrounding areas (Figure 7). Elevated SST in Key Region I or the LST in Key Region II alone intensify precipitation, while their combined effects lead to even higher levels of precipitation in the UAE (Figure 7d).

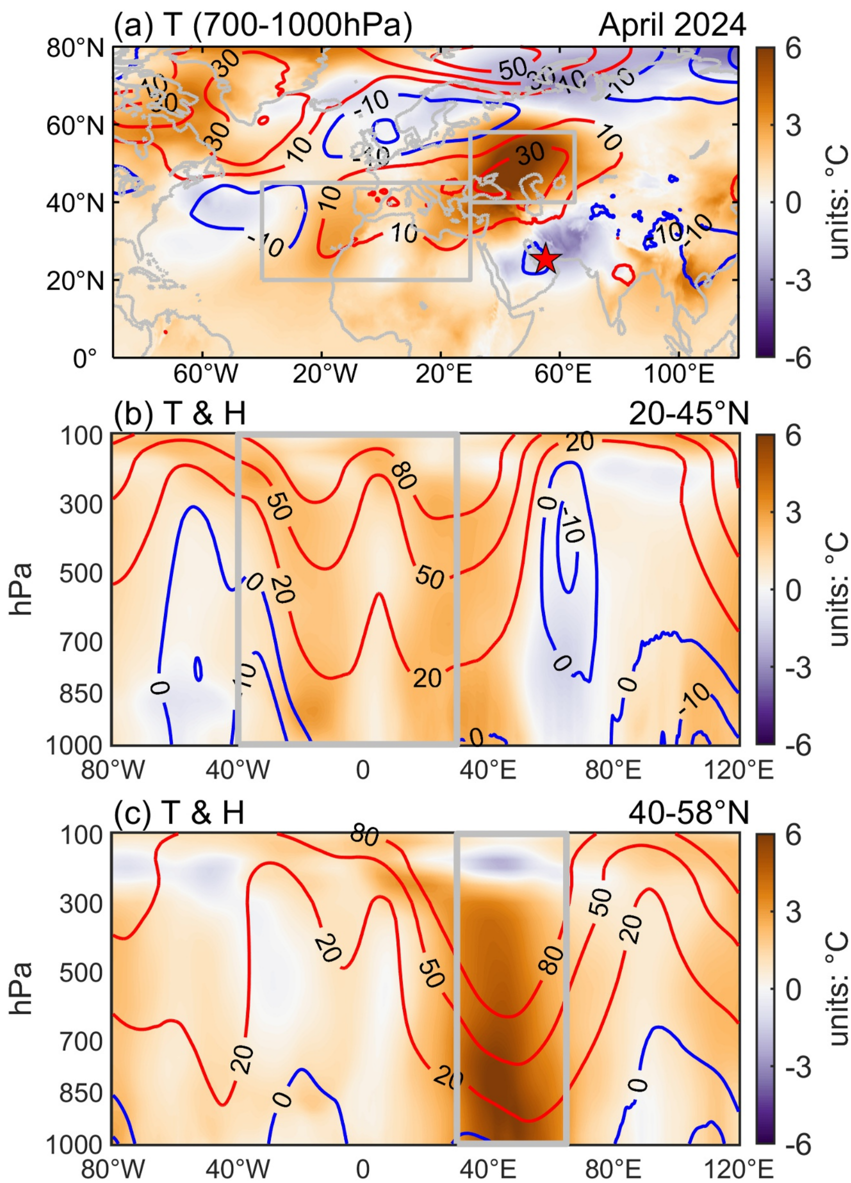

Figure 8. The heating effects of the sea surface and land surface on the atmosphere. (a) Distribution of temperature anomalies averaged between 1,000 and 700 hPa in April 2024, relative to the climatological mean in April of 1991–2020 (shading and contour; units: °C). (b) Longitude-pressure vertical cross-section of temperature anomaly (shading; units: °C) and geopotential height (contour; units: gpm) averaged between 20°N and 45°N. (c) Longitude-pressure vertical cross-section of temperature anomaly (shading; units: °C) and geopotential height (contour; units: gpm) averaged between 40°N and 58°N.

To quantitatively examine the relationship between surface temperatures, atmospheric circulation, and precipitation, we utilized the geopotential height at 500 hPa over the region of interest as a low-pressure index (Table 1). Results indicate that SST in Key Region I is negatively correlated with the geopotential height over the UAE (correlation coefficient = −0.14), which in turn negatively correlates with local precipitation (correlation coefficient = −0.54). As a result, SST in Key Region I shows a positive correlation with precipitation in the UAE (correlation coefficient = 0.22). Similarly, it is observed that the LST in Key Region II exhibits correlation coefficients of 0.26 with precipitation in the UAE and −0.38 with the low-pressure index. These results further verified that the remote influence of these two key regions on UAE precipitation is modulated by an anomalous wave pattern, accompanied by a low-pressure cyclone over the Arabian Peninsula, thus generating favorable dynamic and moisture conditions conducive to precipitation.

Table 1
Pearson Correlation Coefficients Among the SST, LST, Low-Pressure Index, and Precipitation

	SST	Low-pressure index	Precipitation
SST	1	−0.14	0.22*
Low-pressure index		1	−0.54***
Precipitation			1
	LST	**Low-pressure index**	**Precipitation**
LST	1	−0.38***	0.26**
Low-pressure index		1	−0.54***
Precipitation			1

Note. *, **, *** represent significance at the 90%, 95%, and 99% levels, respectively. All correlation coefficients are based on 74 years of data (1951–2024).

The change in atmospheric circulation caused by SST/LST anomalies is a nonlinear process; therefore, to further validate the linear results from a different perspective, we conducted additional composite analysis. Based on standardized anomalies (±1.5σ), we categorized the extreme warm and cold SST/LST events and compared the corresponding atmospheric circulation and precipitation fields (Figure S5 in Supporting Information S1). The results clearly show that warm SST/LST anomalies are associated with enhanced cyclonic anomalies at 500 hPa and increased precipitation over the UAE, which are consistent with the results obtained from the linear methods. This further supports the reliability of the results obtained from Pearson correlation and linear regression analysis in our study. Meanwhile, we also emphasize that these statistical diagnostics and moderate correlations are not interpreted as a causal proof by itself. Next, we will provide a substantial dynamic pathway for these statistical relationships by analyzing thermal forcings, Rossby wave propagation and break.

To explore how surface temperature anomalies induce atmospheric circulation conducive to precipitation in the UAE, we further analyzed the thermal effects of surface temperature on the atmosphere. As illustrated in Figure 8a, increased SST and LST induce warming in the lower troposphere, with atmospheric temperature anomalies mirroring those observed at the surface. Longitude-pressure cross sections also indicate that the thermal forcing linked to surface temperatures in these two key regions has heated the atmosphere, leading to anomalously high temperatures extending up to 200 hPa (Figures 8b and 8c). Notably, the surface and lower-tropospheric warming over the key regions is consistently accompanied by positive geopotential height anomalies, indicating the development of a warm-core anticyclonic circulation as the local thermodynamic response. These favorable conditions promote the excitation of Rossby waves (Dong et al., 2023; Hu et al., 2018; Rodrigues et al., 2019; Tang et al., 2024). Therefore, the anomalous high-pressure system induced by thermal forcing over the key regions, combined with the anomalous low-pressure systems upstream and downstream, closely corresponds to the low-high-low pressure anomaly observed in Figure 6a. In Section 3.3, we will analyze how this wave pattern facilitated extreme precipitation in the UAE.

3.3. Propagation and Breaking of Rossby Waves

To establish the remote physical linkage between SST/LST and atmospheric circulation over the UAE, we investigated the propagation characteristics of Rossby waves induced by SST and LST anomalies through horizontal WAF and stream function analysis. The distribution of WAF for April 2024 reveals pronounced Rossby wave activity propagating from the eastern North Atlantic and Eastern Europe toward the UAE (Figure 9a). These propagations occur along two main pathways: one propagates eastward from the eastern North Atlantic, traversing North Africa and the Mediterranean before reaching the Arabian Peninsula, while the other pathway extends southeastward from Eastern Europe, passing through the Black and Caspian Seas, ultimately arriving in Southwest Asia. In particular, an analysis of the WAF during the intense precipitation event reveals patterns similar to those observed in April but with markedly enhanced wave intensity and clearer propagation characteristics (Figure 9b). The distributions of RWS and divergent winds closely correspond to the previously described wave propagation, with negative centers of RWS (divergent winds) observed over the eastern North Atlantic and central Mediterranean, suggesting these as the source regions for the Rossby waves (Figure 9c). Notably, when these two Rossby waves converged over the northeastern Arabian Peninsula, a discontinuity in the WAF emerged, indicating a weakening or cessation of energy dispersion rather than transmission further eastward. This implies that the Rossby wave may have broken at this point, resulting in the concentration and dissipation of wave energy locally, and thereby establishing a dynamically favorable environment for the extreme precipitation event. Such phenomena are often associated with the subtropical jet, complex topography, and diabatic heating feedbacks, which can intensify wave deformation by altering the PV structure (Grams et al., 2011; Hoskins & Ambrizzi, 1993; Martius et al., 2008; Postel & Hitchman, 1999; Rivière, 2009).

Previous studies have shown that RWB is a critical atmospheric driver of precipitation in global arid regions, contributing to up to 90% of daily precipitation extremes in areas situated equatorward and downstream of mid-latitude storm tracks (de Vries et al., 2024). Additional studies have confirmed a connection between RWB and

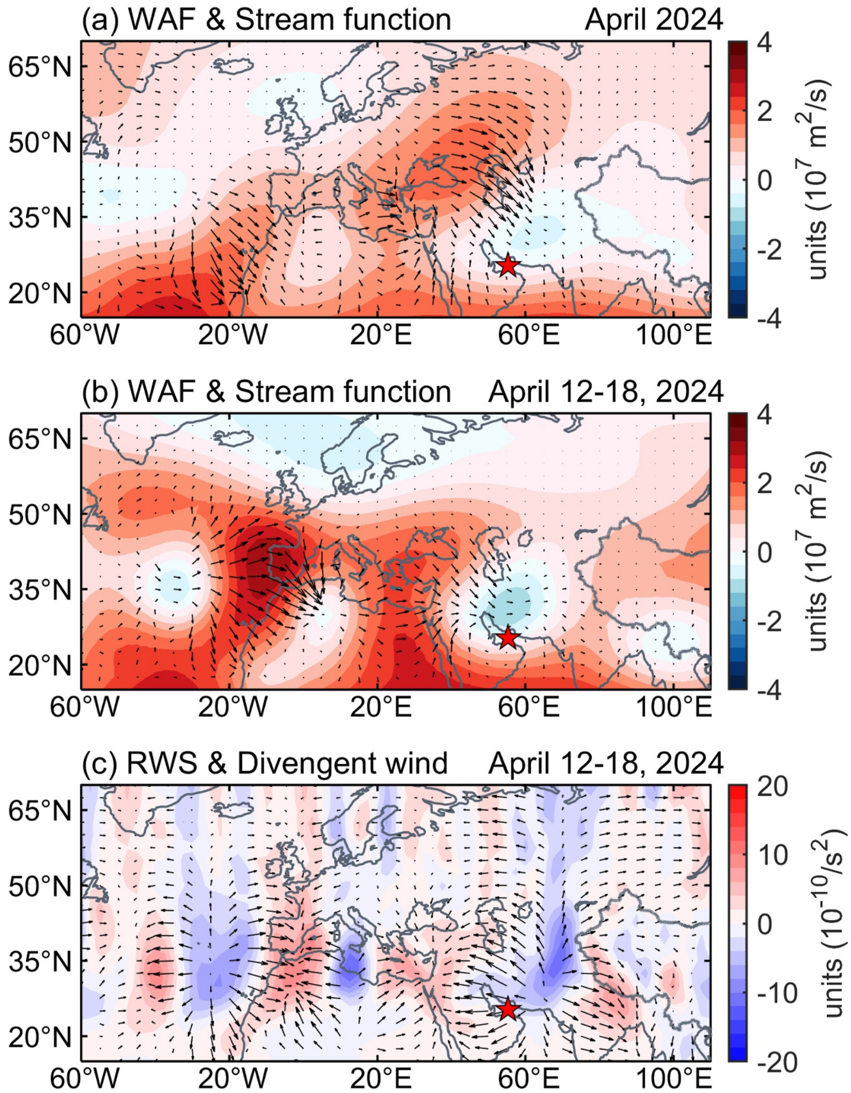

Figure 9. The propagation and sources of Rossby waves. (a) The spatial distribution of wave activity flux (WAF; vectors; unit: m^2/s^2) and stream function anomaly (shading; unit: 10^7 m^2/s) at 200 hPa in April 2024. (b) The same as (a), but during 12–18 April 2024. (c) The spatial distribution of Rossby wave source (RWS; shading; unit: $10^{-10}/s^2$) and divergent wind (vectors; unit: m/s) at 200 hPa during 12–18 April 2024.

extreme precipitation events over the Arabian Peninsula, indicating that these precipitation extremes are linked to PV intrusion, as well as the amplification and breaking of Rossby waves (de Vries et al., 2016, 2018; Kumar et al., 2015; Tuel et al., 2021). In this study, Rossby wave breaking is identified based on the formation of PV streamers on the dynamical tropopause. Figure 10 illustrates the daily distribution of PV contours at 250 hPa during this extreme event. On April 16, we detected a pronounced meridional folding of PV contours over the Arabian Peninsula, and this PV streamer was identified as an RWB event. The equatorward intrusion of high-PV air from the mid-latitudes at the upper troposphere indicates mid-latitude forcing penetrating into lower latitudes through upper-level troughs, leading to intense mixing between high- and low-latitude air masses.

Specifically, RWB directly modulates the circulation through dynamic processes. When the Rossby wave broke on 16 April, the associated upper-tropospheric PV intrusion and jet deformation led to enhanced upper-level divergence (Figures 3a and 3b; Figure S6 in Supporting Information S1). This dynamical configuration induced ascending motion and low-level convergence (Figure S6 in Supporting Information S1), creating a dynamically forced lifting environment conducive to convective initiation, which is consistent with the spatio-temporal distribution of deep convection activity observed on 16 April (Figures 11c and 11h). Meanwhile, regions

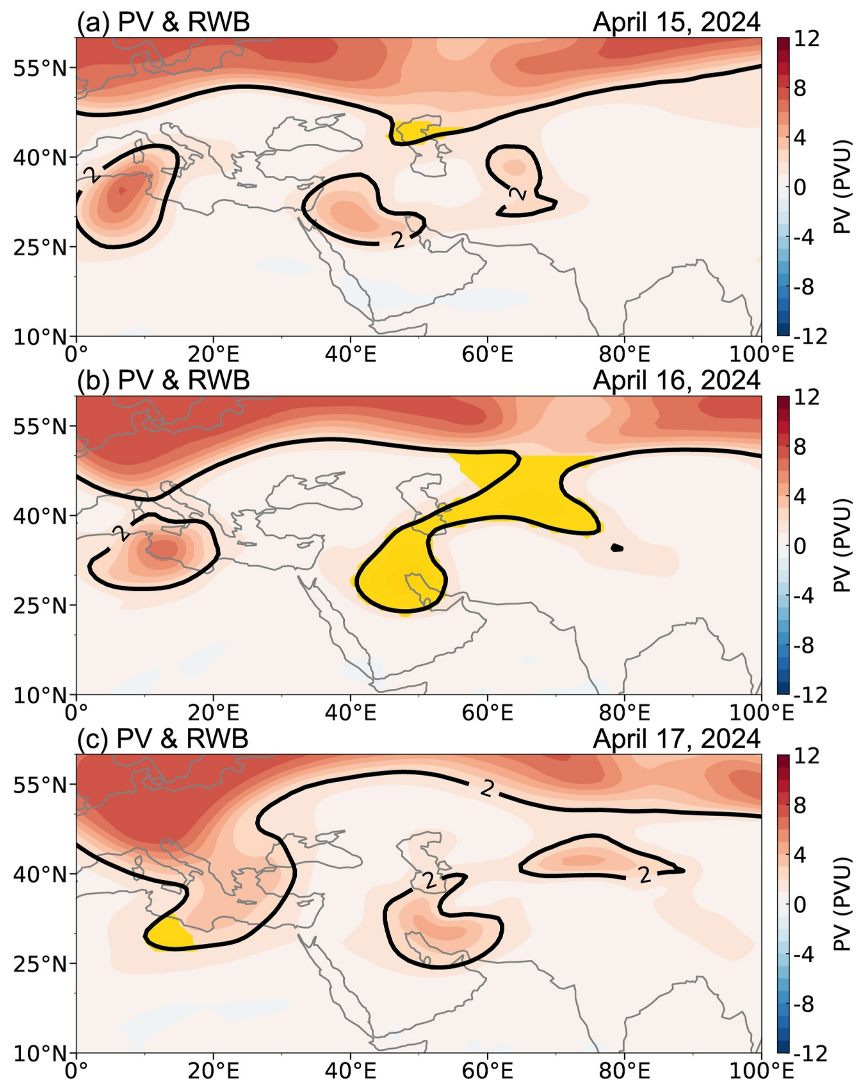

Figure 10. A pronounced RWB phenomenon occurred on 16 April 2024. Spatial distribution of PV (shading; unit: PVU, 1 PVU = 10^{-6} K·m^2·kg^{-1}·s^{-1}) at 250 hPa for (a) −1, (b) 0, and (c) +1 days relative to the UAE extreme precipitation event on 16 April 2024. The black solid line represents the 2 PVU contour. The gold shading highlights the PV streamer identified as a Rossby wave breaking (RWB) event.

of reduced static stability and elevated CAPE exhibit a broad spatial consistency downstream of the upper-level PV streamer, with CAPE values exceeding 1,500 J kg^{-1} (Figures 11a and 11b; Sian et al., 2025). Figure 11g further shows that enhanced CAPE and reduced static stability were already present prior to the occurrence of RWB, while the thermodynamic instability further intensified during the RWB event on 16 April. This additional enhancement can be attributed to dynamic processes associated with RWB. When RWB induces a large-scale ascent, moist air is lifted and condensation occurs, leading to latent heat release that further amplifies local thermodynamic instability. This process is manifested by an upward bulging of isentropic surfaces beneath the upper-level PV anomaly, with the region of reduced static stability situated directly underneath the PV streamer (Figure 11d). In addition, on April 16, pronounced moisture convergence occurred over the study area, with specific humidity exceeding 12 g/kg at 850 hPa over the UAE (Figures 11e and 11f). Thus, the impact of RWB on this extreme precipitation event is manifested in its role as a large-scale dynamical trigger and organizer of convection, together with the amplification of a preconditioned thermodynamic instability through RWB-induced dynamical adjustment, ultimately creating a more favorable environment for deep convection. These findings are consistent with previous studies, as upper-level PV anomalies can dynamically induce upward motion and adjust thermodynamic instability (Funatsu & Waugh, 2008; Hoskins et al., 1985; Sprenger et al., 2010). Consequently,

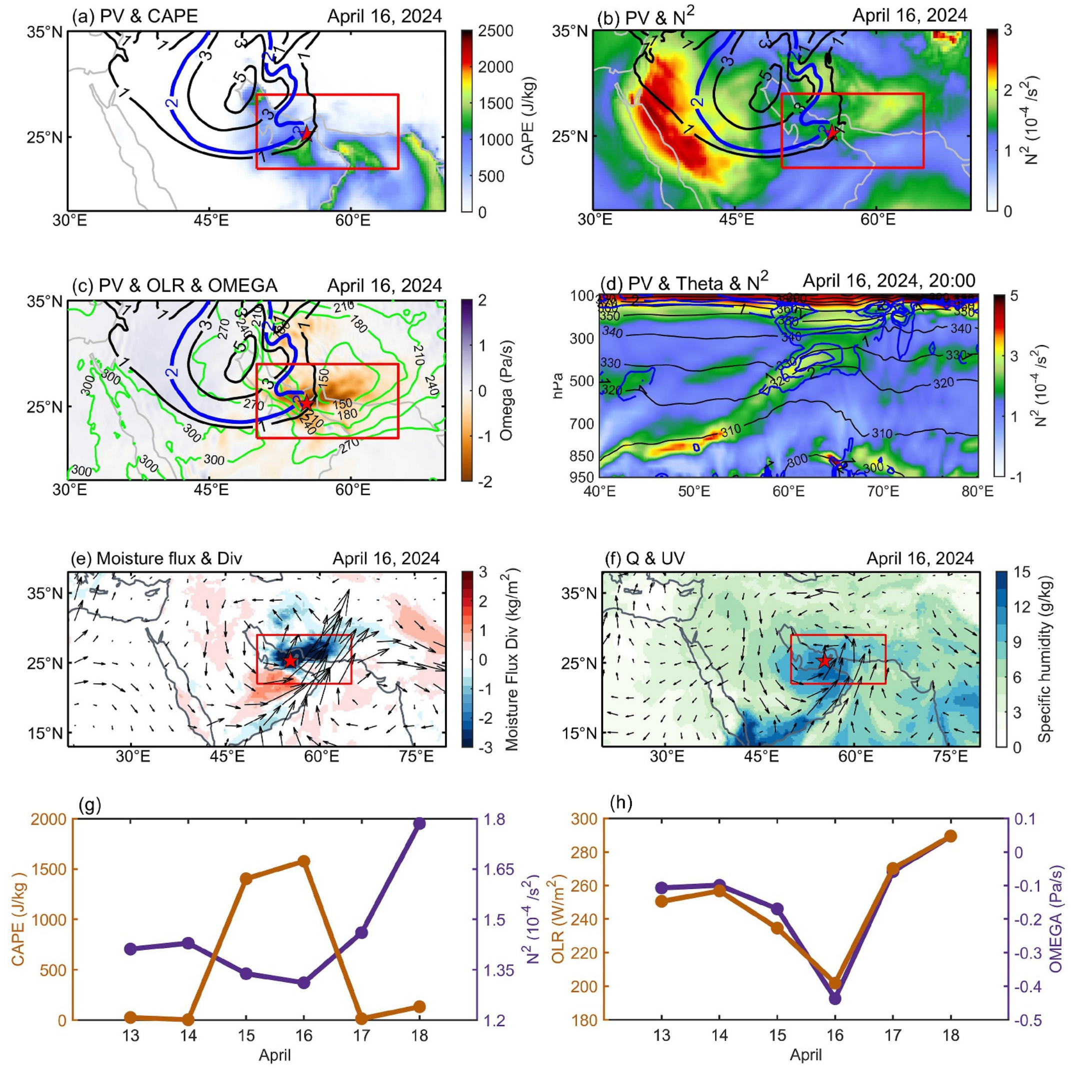

Figure 11. Rossby wave breaking drive the extreme Precipitation on 16 April 2024. (a) CAPE field (shading; unit: $J \cdot kg^{-1}$) and PV field (black line; unit: PVU, 1 PVU = 10^{-6} $K \cdot m^2 \cdot kg^{-1} \cdot s^{-1}$) at the 250 hPa. (b) The index of static stability (Brunt-Väisälä Frequency, N^2; shading; unit: $10^{-4} \cdot s^{-2}$) at 650 hPa and PV field (black line; unit: PVU) at the 250 hPa. (c) OMEGA distribution (shading; unit: $Pa \cdot s^{-1}$) at 500 hPa, OLR (green line; units: W/m^2) and PV field (black line; unit: PVU) at the 250 hPa. (d) Longitude-pressure vertical cross section of N^2 (shading; unit: $10^{-4} \cdot s^{-2}$), potential temperature (Theta; black line; unit: K), and PV (bold blue line; unit: PVU) at 25°N. (e) The vertically integrated water vapor flux (vector) and divergence (shading; units: $kg \cdot m^2$). (f) The specific humidity (shading; units: $g \cdot kg^{-1}$) and wind field (vector) at 850 hPa. (g) Time series of CAPE (brown line; unit: $J \cdot kg^{-1}$) and N^2 (purple line; unit: $10^{-4} \cdot s^{-2}$) over study area. (h) Time series of outgoing longwave radiation (OLR; brown line; unit: W/m^{-2}) and vertical velocity (OMEGA; purple line; unit: Pa/s) over study area.

we propose that RWB acted as a key atmospheric trigger and organizer of this record-breaking extreme precipitation.

4. Conclusions and Discussions

An unprecedented extreme precipitation event struck the hyper-arid UAE in April 2024, causing widespread disruption. Despite its vulnerability, desert rainstorms in this region remain poorly understood. The event peaked on April 16, with precipitation anomalies exceeding 3,000% of the climatological mean, making it the most extreme event on record. Favorable circulation patterns facilitated its occurrence (Figure 12): a split Middle East jet stream enhanced upper-level divergence, while a deep trough developed into an Arabian low vortex, promoting low-level wind convergence and moisture transport from the Arabian and Red Seas. Exceptionally high

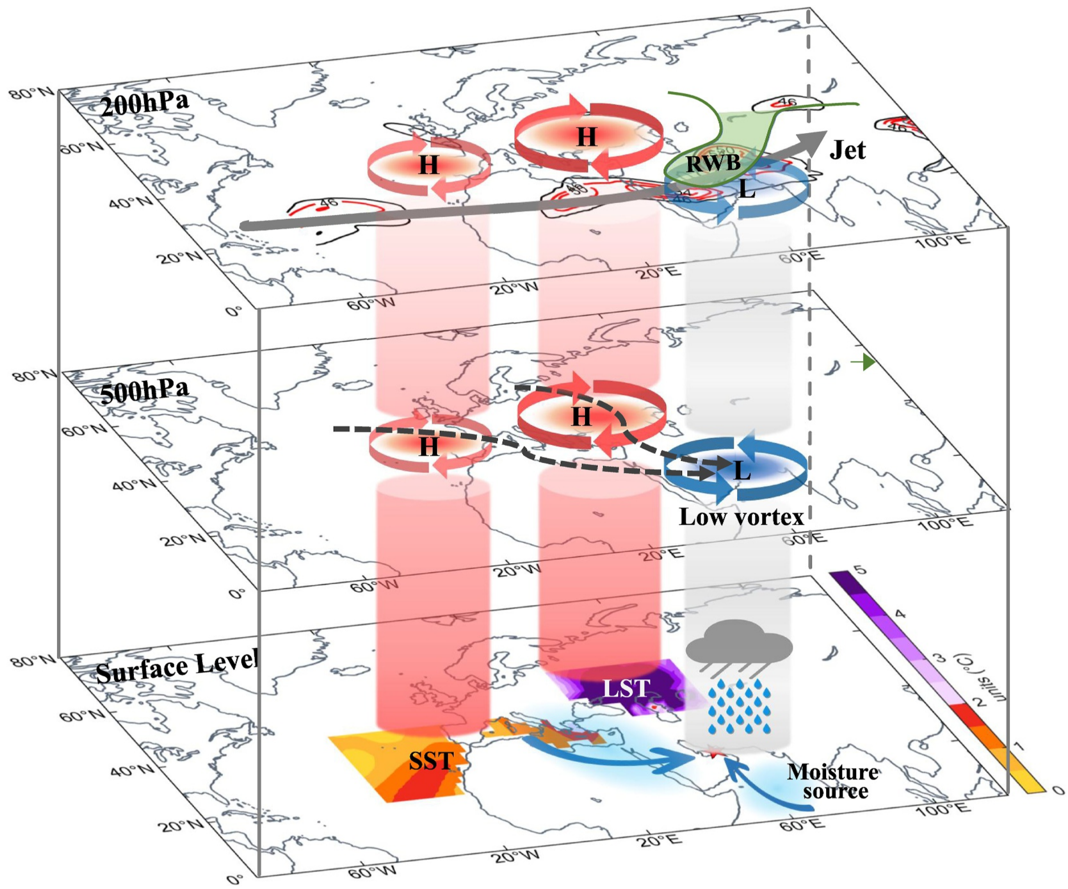

Figure 12. Schematic diagram illustrating the physical mechanism of the UAE extreme precipitation event. At the surface level, shading represents anomalous SST and LST, light blue areas indicate moisture sources, and blue arrows show moisture transport. At 500 hPa, H and L denote high- and- low pressure systems, and the black dashed line marks the Rossby wave propagating path. At 200 hPa, H and L again represent high- and- low pressure systems; black contours denote regions with wind speed exceeding 40 m/s, red contours outline the jet core (≥46 m/s), the gray arrow shows the jet axis, and the green shading highlights RWB.

SST in the eastern North Atlantic–Mediterranean and LST in Eastern Europe reached historical maxima and showed significant positive correlations with UAE precipitation. Their combined thermal anomalies triggered large-scale Rossby waves that propagated downstream, amplifying and breaking over the UAE and surrounding areas. This process strengthened upper-level dynamical forcing and vertical motion and acted to further amplify an already favorable thermodynamic environment, ultimately creating conditions conducive to extreme rainfall. Overall, these findings highlight that remote ocean–atmosphere and land–atmosphere interactions jointly modulated the atmospheric circulation, with RWB serving as the dominant dynamical trigger of this record-breaking event.

It should be noted that, while RWB is identified here as the dominant dynamical trigger of this event, our interpretation is based on physically consistent dynamical diagnostics rather than a strict quantitative causal attribution. A fully quantitative causal attribution, such as RWB sensitivity experiments or robust statistics across multiple events, would require dedicated modeling experiments or a multi-event framework and is beyond the scope of the present single-case study. Beyond this primary mechanism, we further evaluated additional processes that could have influenced the event, including atmospheric rivers and land–atmosphere feedback. Previous studies highlighted the critical role of atmospheric rivers (ARs) in transporting moisture and intensifying extreme precipitation in this region, with their frequency and intensity projected to increase under global warming (Espinoza et al., 2018; Francis et al., 2024; Massoud et al., 2019; Wang et al., 2023). Our analysis confirms the presence of a well-defined AR that efficiently transported moisture from the Arabian Sea to the rainfall region, serving as the primary moisture pathway (Figure S7 in Supporting Information S1). Meanwhile, the hyper-arid land surface conditions in the UAE constrained land-atmosphere feedbacks, as shown by the temporal evolution and correlation analyses of latent and sensible heat fluxes and the evaporative fraction, which primarily responded to rainfall rather than preconditioning the event (Figures S8–S11; Table S1 in Supporting Information S1). Collectively, these results suggest that while multiple processes interacted during the event, RWB provided the key dynamic link integrating remote forcing, convection, and moisture transport.

Recent studies have also shown that global warming induced by anthropogenic activity, including greenhouse gas emissions, land-use changes, and urbanization, has been increasingly associated with the intensification of extreme weather events (Findell et al., 2017; Li et al., 2023; Qian et al., 2022; Touma et al., 2021; Zhou et al., 2023). In this study, the anomalous warming in the North Atlantic-Mediterranean and Eastern Europe, which triggered the Rossby waves responsible for the UAE extreme precipitation, also exhibited a detectable anthropogenic signal consistent with global warming patterns (Hegerl et al., 2011; Jones et al., 2013; Terray, 2012; Twardosz et al., 2021). While our analysis does not explicitly attribute this extreme event to human activities, we recognize that anthropogenic climate change may have intensified the Rossby wave forcing and subsequent precipitation extremes. Therefore, future work using climate model experiments would be valuable to quantitatively assess the contributions of anthropogenic forcing to such events, as well as to examine long-term trends in Rossby wave breaking over arid regions under continued global warming.

In addition, the response of atmospheric circulation and precipitation to surface thermal forcing is nonlinear due to threshold behavior in convection (Graham & Barnett, 1987), background-state dependence (Lau & Nath, 2000), and the nonlinear dynamics of Rossby wave propagation and breaking (McIntyre & Palmer, 1983). While linear statistical methods are useful for establishing the broad relationship and quantifying the first-order response in this study, we also acknowledge the limitations of linear methods in fully capturing these nonlinear behaviors, and future work should incorporate nonlinear or machine-learning approaches to improve understanding and prediction of extreme precipitation in hyper-arid regions.

Conflict of Interest

The authors declare no conflicts of interest relevant to this study.

Availability Statement

ERA5 reanalysis data are available from https://cds.climate.copernicus.eu/datasets. The monthly SST is available from NOAA Extended Reconstructed Sea Surface Temperature, version 5 (ERSST.v5, https://psl.noaa.gov/data/gridded/data.noaa.ersst.v5.html). Figures in this manuscript were made with MATLAB version 2020a, and this software is available from www.mathworks.com/ (The Math Works, Inc, 2020).

Acknowledgments
This work was jointly supported by the National Natural Science Foundation of China (42522503 and 423B2501), the Lanzhou Special Fund for Talent Program, and the Gansu Leading Talent Development Fund.

References

AghaKouchak, A., Chiang, F., Huning, L. S., Love, C. A., Mallakpour, I., Mazdiyasni, O., et al. (2020). Climate extremes and compound hazards in a warming world. *Annual Review of Earth and Planetary Sciences*, *48*(1), 519–548. https://doi.org/10.1146/annurev-earth-071719-055228

Aizen, E. M., Aizen, V. B., Melack, J. M., Nakamura, T., & Ohta, T. (2001). Precipitation and atmospheric circulation patterns at mid-latitudes of Asia. *International Journal of Climatology*, *21*(5), 535–556. https://doi.org/10.1002/joc.626

Allen, G., Vaughan, G., Brunner, D., May, P. T., Heyes, W., Minnis, P., & Ayers, J. K. (2008). Modulation of tropical convection by breaking Rossby waves. *Quarterly Journal of the Royal Meteorological Society*, *135*(638), 125–137. https://doi.org/10.1002/qj.349

Almheiri, K. B., Rustum, R., Wright, G., & Adeloye, A. J. (2024). The necessity of updating IDF curves for the Sharjah Emirate, UAE: A comparative analysis of 2020 IDF values in light of recent urban flooding (April 2024). *Water*, *16*(18), 2621. https://doi.org/10.3390/w16182621

Biyo, T., Kunchala, R. K., Kumar, K. N., Singh, B. B., & Yesubabu, V. (2024). Surface temperature modulations induced by Rossby Wave Breaking over Indian region. *Environmental Research Communications*, *6*(10), 105017. https://doi.org/10.1088/2515-7620/ad832f

Chowdhury, R., Mohamed, M. M. A., & Murad, A. (2016). Variability of extreme hydro-climate parameters in the North-Eastern Region of United Arab Emirates. *Procedia Engineering*, *154*, 639–644. https://doi.org/10.1016/j.proeng.2016.07.563

Cullen, H. M., & deMenocal, P. B. (2000). North Atlantic influence on Tigris-Euphrates streamflow. *International Journal of Climatology*, *20*(8), 853–863. https://doi.org/10.1002/1097-0088(20000630)20:8<853::AID-JOC497>3.0.CO;2-M

Cullen, H. M., Kaplan, A., Arkin, P. A., & deMenocal, P. B. (2002). Impact of the North Atlantic Oscillation on Middle Eastern climate and streamflow. *Climatic Change*, *55*(3), 315–338. https://doi.org/10.1023/A:1020518305517

De Vries, A. J., Armon, M., Klingmüller, K., Portmann, R., Röthlisberger, M., & Domeisen, D. I. (2024). Breaking Rossby waves drive extreme precipitation in the world's arid regions. *Communications Earth & Environment*, *5*(1), 493. https://doi.org/10.1038/s43247-024-01633-y

De Vries, A. J., Feldstein, S. B., Riemer, M., Tyrlis, E., Sprenger, M., Baumgart, M., et al. (2016). Dynamics of tropical–extratropical interactions and extreme precipitation events in Saudi Arabia in autumn, winter and spring. *Quarterly Journal of the Royal Meteorological Society*, *142*(697), 1862–1880. https://doi.org/10.1002/qj.2781

De Vries, A. J., Ouwersloot, H. G., Feldstein, S. B., Riemer, M., El Kenawy, A. M., McCabe, M. F., & Lelieveld, J. (2018). Identification of tropical–extratropical interactions and extreme precipitation events in the middle east based on potential vorticity and moisture transport. *Journal of Geophysical Research: Atmospheres*, *123*(2), 861–881. https://doi.org/10.1002/2017JD027587

Dominguez, F., Hu, H., & Martinez, J. A. (2020). Two-layer dynamic recycling model (2L-DRM): Learning from moisture tracking models of different complexity. *Journal of Hydrometeorology*, *21*(1), 3–16. https://doi.org/10.1175/JHM-D-19-0101.1

Dominguez, F., Kumar, P., Liang, X. Z., & Ting, M. (2006). Impact of atmospheric moisture storage on precipitation recycling. *Journal of Climate*, *19*(8), 1513–1530. https://doi.org/10.1175/JCLI3691.1

Donat, M. G., Lowry, A. L., Alexander, L. V., O'Gorman, P. A., & Maher, N. (2016). More extreme precipitation in the world's dry and wet regions. *Nature Climate Change*, *6*(5), 508–513. https://doi.org/10.1038/nclimate2941

Dong, W., Jia, X., & Wu, R. (2023). Impact of summer Tibetan Plateau snow cover on the variability of concurrent compound heatwaves in the Northern Hemisphere. *Environmental Research Letters*, *19*(1), 014057. https://doi.org/10.1088/1748-9326/ad1435

Duan, R., Huang, G., Zhou, X., Lu, C., & Tian, C. (2023). Record-breaking heavy rainfall around Henan Province in 2021 and future projection of extreme conditions under climate change. *Journal of Hydrology*, *625*, 130102. https://doi.org/10.1016/j.jhydrol.2023.130102

Espinoza, V., Waliser, D. E., Guan, B., Lavers, D. A., & Ralph, F. M. (2018). Global analysis of climate change projection effects on atmospheric rivers. *Geophysical Research Letters*, *45*(9), 4299–4308. https://doi.org/10.1029/2017GL076968

Ferreira, S. (2024). Extreme weather events and climate change: Economic impacts and adaptation policies. *Annual Review of Resource Economics*, *16*(1), 207–231. https://doi.org/10.1146/annurev-resource-101623-095314

Findell, K. L., Berg, A., Gentine, P., Krasting, J. P., Lintner, B. R., Malyshev, S., et al. (2017). The impact of anthropogenic land use and land cover change on regional climate extremes. *Nature Communications*, *8*(1), 989. https://doi.org/10.1038/s41467-017-01038-w

Fonseca, R., Francis, D., Nelli, N., & Thota, M. (2021). Climatology of the heat low and the intertropical discontinuity in the Arabian Peninsula. *International Journal of Climatology*, *42*(2), 1092–1117. https://doi.org/10.1002/essoar.10507443.1

Francis, D., Fonseca, R., Bozkurt, D., Nelli, N., & Guan, B. (2024). Atmospheric river rapids and their role in the extreme rainfall event of April 2023 in the Middle East. *Geophysical Research Letters*, *51*(12), e2024GL109446. https://doi.org/10.1029/2024GL109446

Funatsu, B. M., & Waugh, D. W. (2008). Connections between potential vorticity intrusions and convection in the Eastern Tropical Pacific. *Journal of the Atmospheric Sciences*, *65*(3), 987–1002. https://doi.org/10.1175/2007JAS2248.1

Gong, H., Ma, K., Wang, L., & Chen, W. (2024). Attribution of the record-breaking extreme cold event over Northern East Asia in December 2023. *Geophysical Research Letters*, *51*(23), e2024GL112568. https://doi.org/10.1029/2024GL112568

Graham, N. E., & Barnett, T. P. (1987). Sea surface temperature, surface wind divergence, and convection over tropical oceans. *Science*, *238*(4827), 657–659. https://doi.org/10.1126/science.238.4827.657

Grams, C. M., Wernli, H., Böttcher, M., Čampa, J., Corsmeier, U., Jones, S. C., et al. (2011). The key role of diabatic processes in modifying the upper-tropospheric wave guide: A North Atlantic case-study. *Quarterly Journal of the Royal Meteorological Society*, *137*(661), 2174–2193. https://doi.org/10.1002/qj.891

Guan, X., & Huang, J. (2024). Constructing semi-arid ecological barriers to prevent desertification. *The Innovation Geoscience*, *2*(2), 100067. https://doi.org/10.59717/j.xinn-geo.2024.100067

Guan, X., Sun, W., Kong, X., Zhang, F., Huang, J., & He, Y. (2023). Response of fatal landslides to precipitation over the Chinese Loess Plateau under global warming. *Frontiers in Earth Science*, *11*, 1146724. https://doi.org/10.3389/feart.2023.1146724

Hegerl, G., Luterbacher, J., González-Rouco, F., Tett, S. F., Crowley, T., & Xoplaki, E. (2011). Influence of human and natural forcing on European seasonal temperatures. *Nature Geoscience*, *4*(2), 99–103. https://doi.org/10.1038/ngeo1057

Hersbach, H., Bell, B., Berrisford, P., Hirahara, S., Horányi, A., Muñoz-Sabater, J., et al. (2020). The ERA5 global reanalysis. *Quarterly Journal of the Royal Meteorological Society*, *146*(730), 1999–2049. https://doi.org/10.1002/qj.3803

Hoskins, B. J., & Ambrizzi, T. (1993). Rossby wave propagation on a realisticlongitudinally varying flow. *Journal of Atmospheric Sciences*, *50*(12), 1661–1671. https://doi.org/10.1175/1520-0469(1993)050%3C1661:RWPOAR%3E2.0.CO;2

Hoskins, B. J., McIntyre, M. E., & Robertson, A. W. (1985). On the use and significance of isentropic potential vorticity maps. *Quarterly Journal of the Royal Meteorological Society*, *111*(470), 877–946. https://doi.org/10.1002/qj.49711147002

Hsu, P. C., Xie, J., Lee, J. Y., Zhu, Z., Li, Y., Chen, B., & Zhang, S. (2023). Multiscale interactions driving the devastating floods in Henan Province, China during July 2021. *Weather and Climate Extremes*, *39*, 100541. https://doi.org/10.1016/j.wace.2022.100541

Hu, X., Cai, M., Yang, S., & Wu, Z. (2018). Delineation of thermodynamic and dynamic responses to sea surface temperature forcing associated with El Niño. *Climate Dynamics*, *51*(11–12), 4329–4344. https://doi.org/10.1007/s00382-017-3711-0

Huang, B., Thorne, P. W., Banzon, V. F., Boyer, T., Chepurin, G., Lawrimore, J. H., et al. (2017). Extended reconstructed sea surface temperature, Version 5 (ERSSTv5): Upgrades, validations, and intercomparisons. *Journal of Climate*, *30*(20), 8179–8205. https://doi.org/10.1175/JCLI-D-16-0836.1

Huang, J., Li, Y., Fu, C., Chen, F., Fu, Q., Dai, A., et al. (2017). Dryland climate change: Recent progress and challenges. *Reviews of Geophysics*, *55*(3), 719–778. https://doi.org/10.1002/2016RG000550

Huang, S. H., Wen, Z. P., Chen, X. D., Guo, Y. Y., & Wang, Z. W. (2022). The Henan extreme rainfall in July 2021: Modulation of the northward-shift monsoon trough on the synoptic-scale wave train. *Advances in Climate Change Research*, *13*(6), 819–825. https://doi.org/10.1016/j.accre.2022.11.001

Jones, G. S., Stott, P. A., & Christidis, N. (2013). Attribution of observed historical near–surface temperature variations to anthropogenic and natural causes using CMIP5 simulations. *Journal of Geophysical Research: Atmospheres*, *118*(10), 4001–4024. https://doi.org/10.1002/jgrd.50239

Kumar, K. N., Entekhabi, D., & Molini, A. (2015). Hydrological extremes in hyperarid regions: A diagnostic characterization of intense precipitation over the Central Arabian Peninsula. *Journal of Geophysical Research: Atmospheres*, *120*(5), 1637–1650. https://doi.org/10.1002/2014JD022341

Lau, N. C., & Nath, M. J. (2000). Impact of ENSO on the variability of the Asian–Australian monsoons as simulated in GCM experiments. *Journal of Climate*, *13*(24), 4287–4309. https://doi.org/10.1175/1520-0442(2000)013<4287:IOEOTV>2.0.CO;2

Li, W., Sun, B., Wang, H., Zhou, B., Li, H., Xue, R., et al. (2023). Anthropogenic impact on the severity of compound extreme high temperature and drought/rain events in China. *npj Climate and Atmospheric Science*, *6*(1), 79. https://doi.org/10.1038/s41612-023-00413-3

Martius, O., Schwierz, C., & Davies, H. C. (2008). Far-upstream precursors of heavyprecipitation events on the Alpine south-side. *Quarterly Journal of the Royal Meteorological Society: A Journal of the Atmospheric Sciences, Appliedmeteorology and Physical Oceanography*, *134*(631), 417–428. https://doi.org/10.1002/qj.229

Massoud, E. C., Espinoza, V., Guan, B., & Waliser, D. E. (2019). Global climate model ensemble approaches for future projections of atmospheric rivers. *Earth's Future*, *7*(10), 1136–1151. https://doi.org/10.1029/2019EF001249

McIntyre, M. E., & Palmer, T. N. (1983). Breaking planetary waves in the stratosphere. *Nature*, *305*(5935), 593–600. https://doi.org/10.1038/305593a0

McIntyre, M. E., & Palmer, T. N. (1985). A note on the general concept of wave breaking for Rossby and gravity waves. *Pure and Applied Geophysics*, *123*(6), 964–975. https://doi.org/10.1007/BF00876984

Nelli, N. R., Francis, D., Fonseca, R., Abida, R., Weston, M., Wehbe, Y., & Al Hosary, T. (2021). The atmospheric controls of extreme convective events over the southern Arabian Peninsula during the spring season. *Atmospheric Research*, *262*, 105788. https://doi.org/10.1016/j.atmosres.2021.105788

Nie, Y., & Sun, J. (2022). Moisture sources and transport for extreme precipitation over Henan in July 2021. *Geophysical Research Letters*, *49*(4), e2021GL097446. https://doi.org/10.1029/2021GL097446

Nielsen-Gammon, J. W. (2001). A visualization of the global dynamic tropopause. *Bulletin of the American Meteorological Society*, *82*(6), 1151–1167. https://doi.org/10.1175/1520-0477(2001)082<1151:AVOTGD>2.3.CO;2

Niranjan Kumar, K., & Ouarda, T. B. M. J. (2014). Precipitation variability over UAE and global SST teleconnections. *Journal of Geophysical Research: Atmospheres*, *119*(17). https://doi.org/10.1002/2014JD021724

Niranjan Kumar, K., Ouarda, T. B. M. J., Sandeep, S., & Ajayamohan, R. S. (2016). Wintertime precipitation variability over the Arabian Peninsula and its relationship with ENSO in the CAM4 simulations. *Climate Dynamics*, *47*(7–8), 2443–2454. https://doi.org/10.1007/s00382-016-2973-2

Nyarko, I. K. (2024). The impact of natural disasters on international trade: The potential effects of April 2024 Dubai floods on Ghana's economy. *Business, Management and Economics: Research Progress*, *4*, 64–86. https://doi.org/10.9734/bpi/bmerp/v4/1540

Ouarda, T. B., Charron, C., Kumar, K. N., Marpu, P. R., Ghedira, H., Molini, A., & Khayal, I. (2014). Evolution of the rainfall regime in the United Arab Emirates. *Journal of Hydrology*, *514*, 258–270. https://doi.org/10.1016/j.jhydrol.2014.04.032

Postel, G. A., & Hitchman, M. H. (1999). A climatology of Rossby wave breaking alongthe subtropical tropopause. *Journal of the Atmospheric Sciences*, *56*(3), 359–373. https://doi.org/10.1175/1520-0469(1999)056<0359:ACORWB>2.0.CO;2

Qian, Y., Chakraborty, T. C., Li, J., Li, D., He, C., Sarangi, C., et al. (2022). Urbanization impact on regional climate and extreme weather: Current understanding, uncertainties, and future research directions. *Advances in Atmospheric Sciences*, *39*(6), 819–860. https://doi.org/10.1007/s00376-021-1371-9

Rana, S., Renwick, J., McGregor, J., & Singh, A. (2018). Seasonal prediction of winter precipitation anomalies over Central Southwest Asia: A canonical correlation analysis approach. *Journal of Climate*, *31*(2), 727–741. https://doi.org/10.1175/JCLI-D-17-0131.1

Renwick, J., McGregor, J., & Rana, S. (2015). Precipitation seasonality over the Indian subcontinent: An evaluation of gauge, reanalyses, and satellite retrievals. *Journal of Hydrometeorology*, *16*(2), 631–651. https://doi.org/10.1175/JHM-D-14-0106.1

Rivière, G. (2009). Effect of latitudinal variations in low-level baroclinicity on eddylife cycles and upper-tropospheric wave-breaking processes. *Journal of the Atmospheric Sciences*, *66*(6), 1569–1592. https://doi.org/10.1175/2008JAS2919.1

Rodrigues, R. R., Taschetto, A. S., Sen Gupta, A., & Foltz, G. R. (2019). Common cause for severe droughts in South America and marine heatwaves in the South Atlantic. *Nature Geoscience*, *12*(8), 620–626. https://doi.org/10.1038/s41561-019-0393-8

Sandeep, S., & Ajayamohan, R. S. (2018). Modulation of winter precipitation dynamics over the Arabian Gulf by ENSO. *Journal of Geophysical Research: Atmospheres*, *123*(1), 198–210. https://doi.org/10.1002/2017JD027263

Sardeshmukh, P. D., & Hoskins, B. J. (1988). The generation of global rotational flow by steady idealized tropical divergence. *Journal of the Atmospheric Sciences*, *45*(7), 1228–1251. https://doi.org/10.1175/1520-0469(1988)045<1228:TGOGRF>2.0.CO;2

Sekizawa, S., Nakamura, H., & Kosaka, Y. (2021). Remote influence of the interannual variability of the Australian summer monsoon on wintertime climate in East Asia and the western North Pacific. *Journal of Climate*, *34*(23), 9551–9570. https://doi.org/10.1175/JCLI-D-21-0202.1

Shu, X., Wang, S., Wang, H., Hu, Y., Pang, Y., & Huang, J. (2024). South-North dipole in summer precipitation over Northeast China. *Climate Dynamics*, *62*(7), 6913–6930. https://doi.org/10.1007/s00382-024-07256-5

Sian, K. T. C. L. K., Sagero, P., Kebacho, L. L., & Ongoma, V. (2025). Dubai's record precipitation event of 16 April 2024–A diagnosis. *Atmospheric Research*, *315*, 107924. https://doi.org/10.1016/j.atmosres.2025.107924

Sprenger, M., Fragkoulidis, G., Binder, H., Croci-Maspoli, M., Graf, P., Grams, C. M., et al. (2017). Global climatologies of Eulerian and Lagrangian flow features based on ERA-Interim. *Bulletin of the American Meteorological Society*, *98*(8), 1739–1748. https://doi.org/10.1175/BAMS-D-15-00299.1

Sprenger, M., Martius, O., Schlemmer, L., Schwierz, C., & Twitchett, A. (2010). Disentangling the forcing mechanisms of a heavy precipitation event along the alpine south side using potential vorticity inversion. *Monthly Weather Review*, *138*(6), 2336–2353. https://doi.org/10.1175/2009MWR3202.1

Suman, M., & Maity, R. (2020). Southward shift of precipitation extremes over south Asia: Evidences from CORDEX data. *Scientific Reports*, *10*(1), 6452. https://doi.org/10.1038/s41598-020-63571-x

Sun, Q., Zhang, X., Zwiers, F., Westra, S., & Alexander, L. V. (2021). A global, continental, and regional analysis of changes in extreme precipitation. *Journal of Climate*, *34*(1), 243–258. https://doi.org/10.1175/JCLI-D-19-0892.1

Takaya, K., & Nakamura, H. (2001). A formulation of a phase-independent wave-activity flux for stationary and migratory quasigeostrophic eddies on a zonally varying basic flow. *Journal of the Atmospheric Sciences*, *58*(6), 608–627. https://doi.org/10.1175/1520-0469(2001)058<0608:AFOAPI>2.0.CO;2

Tang, S., Piao, S., Holland, D. M., Kan, F., Wang, T., Yao, T., & Li, X. (2024). Resonance between projected Tibetan Plateau surface darkening and Arctic climate change. *Science Bulletin*, *69*(3), 367–374. https://doi.org/10.1016/j.scib.2023.12.008

Taraphdar, S., Pauluis, O. M., Xue, L., Liu, C., Rasmussen, R., Ajayamohan, R. S., et al. (2021). WRF gray-zone simulations of precipitation over the Middle-East and the UAE: Impacts of physical parameterizations and resolution. *Journal of Geophysical Research: Atmospheres*, *126*(10), e2021JD034648. https://doi.org/10.1029/2021JD034648

Terray, L. (2012). Evidence for multiple drivers of North Atlantic multi-decadal climate variability. *Geophysical Research Letters*, *39*(19). https://doi.org/10.1029/2012GL053046

The Math Works, Inc. (2020). MATLAB (Version 2020a) [Software]. Retrieved from www.mathworks.com/

Touma, D., Stevenson, S., Lehner, F., & Coats, S. (2021). Human-driven greenhouse gas and aerosol emissions cause distinct regional impacts on extreme fire weather. *Nature Communications*, *12*(1), 212. https://doi.org/10.1038/s41467-020-20570-w

Tuel, A., Choi, Y. W., AlRukaibi, D., & Eltahir, E. A. B. (2021). Extreme storms in Southwest Asia (Northern Arabian Peninsula) under current and future climates. *Climate Dynamics*, *58*(5–6), 1509–1524. https://doi.org/10.1007/s00382-021-05975-7

Twardosz, R., Walanus, A., & Guzik, I. (2021). Warming in Europe: Recent trends in annual and seasonal temperatures. *Pure and Applied Geophysics*, *178*(10), 4021–4032. https://doi.org/10.1007/s00024-021-02860-6

Wang, S., Huang, J., Huang, G., Luo, F., Ren, Y., & He, Y. (2022). Enhanced impacts of Indian Ocean Sea surface temperature on the dry/wet variations over Northwest China. *Journal of Geophysical Research: Atmospheres*, *127*(11), e2022JD036533. https://doi.org/10.1029/2022JD036533

Wang, S., Ma, X., Zhou, S., Wu, L., Wang, H., Tang, Z., et al. (2023). Extreme atmospheric rivers in a warming climate. *Nature Communications*, *14*(1), 3219. https://doi.org/10.1038/s41467-023-38980-x

Wernli, H., & Sprenger, M. (2007). Identification and ERA-15 climatology of potential vorticity streamers and cutoffs near the extratropical tropopause. *Journal of the Atmospheric Sciences*, *64*(5), 1569–1586. https://doi.org/10.1175/JAS3912.1

Wilks, D. S. (2019). *Statistical methods in the atmospheric sciences* (4th ed.). Elsevier. https://doi.org/10.1016/C2017-0-03921-6

Yang, R., Zhang, W. K., Gui, S., Tao, Y., & Cao, J. (2019). Rainy season precipitation variation in the Mekong River basin and its relationship to the Indian and East Asian summer monsoons. *Climate Dynamics*, *52*(9), 5691–5708. https://doi.org/10.1007/s00382-018-4471-1

Zeder, J., & Fischer, E. M. (2020). Observed extreme precipitation trends and scaling in Central Europe. *Weather and Climate Extremes*, *29*, 100266. https://doi.org/10.1016/j.wace.2020.100266

Zhang, J., Wang, S., Huang, J., He, Y., & Ren, Y. (2023). The precipitation-recycling process enhanced extreme precipitation in Xinjiang, China. *Geophysical Research Letters*, *50*(15), e2023GL104324. https://doi.org/10.1029/2023GL104324

Zhang, W., & Zhou, T. (2020). Increasing impacts from extreme precipitation on population over China with global warming. *Science Bulletin*, *65*(3), 243–252. https://doi.org/10.1016/j.scib.2019.12.002

Zhang, W., Zhou, T., & Wu, P. (2024). Anthropogenic amplification of precipitation variability over the past century. *Science*, *385*(6707), 427–432. https://doi.org/10.1126/science.adp0212

Zhou, S., Yu, B., & Zhang, Y. (2023). Global concurrent climate extremes exacerbated by anthropogenic climate change. *Science Advances*, *9*(10), eabo1638. https://doi.org/10.1126/sciadv.abo1638